The Contribution of Mesoscale Motions to the Mass and Heat Fluxes of an Intense Tropical Convective System[1]

COLLEEN A. LEARY[2] AND ROBERT A. HOUZE, JR.

Department of Atmospheric Sciences, University of Washington, Seattle 98195

(Manuscript received 31 July 1979, in final form 5 November)

ABSTRACT

The existence of extensive precipitating anvil clouds in intense tropical convection suggests that vertical air motions associated with the anvil clouds play a significant role in the mass and heat budgets of these systems. This paper uses three different sets of assumptions about the water budget of an idealized mesoscale convective system to test the sensitivity of diagnostic calculations of vertical transports of mass and heat to the inclusion or exclusion of anvil clouds and their associated mesoscale vertical air motions. The properties of the mesoscale updraft and downdraft are evaluated using observations and the results of modeling studies. When a mesoscale updraft and downdraft are included in the diagnostic calculations, the profiles of vertical transports of mass and moist static energy are both qualitatively and quantitatively different from the results when mesoscale vertical air motions are excluded. Inclusion of mesoscale vertical motions in the diagnostic calculations leads to smaller upward mass transports below 4 km, larger upward mass transports above 4 km, less cooling below 4 km, and more cooling between 4.5 and 6.5 km than are obtained when mesoscale motions are not included in the calculations. These results imply that the effect of mesoscale vertical air motions on cloud mass flux and net heating profiles should be considered when parameterizing the effects of tropical convection on the larger scale environment.

1. Introduction

Abercromby (1887) was perhaps the first to document the anomalously low surface temperatures observed to the rear of an intense squall line and suggest that they were due to the transport downward of cold air with heavy rain. Humphreys (1914) proposed evaporation of falling rain to be the dominant mechanism for the cooling as well as the source of the downdrafts in large thunderstorms. He also noted two distinct rain areas in the thunderstorm: a primary rain area located close to the ascending air, and a less intense secondary rain area well to the rear of the ascending air and the primary rain area. In the tropics, Hamilton and Archbold (1945) described similar phenomena in squall lines, which they called disturbance lines, and associated the light rain area to the rear of the most intense showers with a deep anvil of altostratus cloud.

Zipser (1969) deduced the presence of an organized mesoscale downdraft driven by the evaporation of falling precipitation beneath the anvil cloud in the rear portion of tropical squall-line systems. He distinguished this mesoscale downdraft, which is several hundred kilometers in horizontal extent, from the convective-scale updrafts and downdrafts (1–10 km in horizontal extent) which occurred at the leading edge of the system. Houze (1977) and Zipser (1977) have shown that similar squall-line systems occurred in the Global Atmospheric Research Program's Atlantic Tropical Experiment (GATE). Zipser and Gautier (1978) and Leary and Houze (1979b) have found evidence for mesoscale downdrafts below anvil clouds in non-squall as well as squall-line mesoscale systems in GATE. Leary and Houze (1979a) examined the horizontally uniform precipitation associated with the anvil clouds in five cases, including both squall and non-squall mesoscale systems and presented calculations based on these cases, which suggest that cooling resulting from the melting of hydrometeors, in addition to evaporative cooling, plays an important role in the initiation and maintenance of mesoscale downdrafts in intense convective systems.

Motivated by Zipser's (1969) study, Brown (1979) constructed a two-dimensional, time-dependent numerical model of a precipitating tropical disturbance, using unfiltered hydrostatic equations, together with parameterizations of cloud microphysics and convective-scale motions. In his experiments, an anvil cloud evolved, and a broad mesoscale downdraft developed as a hydrostatic,

[1] Contribution No. 517 Department of Atmospheric Sciences, University of Washington.

[2] Present affiliation: Atmospheric Science Group, Texas Tech University, Lubbock 79409.

0022-4928/80/040784-13$07.25

© 1980 American Meteorological Society

thermally direct circulation feature, when cooling due to the evaporation of rain falling from the anvil cloud was included in the calculations. Above the mesoscale downdraft, which occurred in the lower troposphere below the base of the anvil cloud, Brown's model produced a mesoscale region of hydrostatic uplift in the anvil cloud layer itself. Thus, the region immediately to the rear of the line of cumulonimbus towers was characterized by a mesoscale updraft located aloft, directly above an evaporatively driven mesoscale downdraft.

The importance of the precipitation falling from the anvil clouds of intense convective systems is indicated by the fact that it accounts for ~40% of the total rainfall observed in GATE (Cheng and Houze, 1979). It seems reasonable, therefore, to believe that the mesoscale updrafts and downdrafts associated with anvil clouds played a significant role in the cloud mass and heat fluxes over the GATE data network. To determine their role quantitatively, diagnostic techniques are needed which can detect the fluxes by the mesoscale drafts. Houze *et al.* (1980), hereafter referred to as H) developed equations for the diagnosis of cloud mass and heat fluxes either from observations of the precipitation fields associated with the clouds (the radar approach) or from large-scale heat budgets (the synoptic approach). Whichever of the two approaches is used, assumptions about cloud water budgets must be made to determine the amount of mesoscale air motion contributing to the fluxes. Previous diagnostic studies (e.g., Yanai *et al.*, 1973; Ogura and Cho, 1973; Johnson, 1976; Houze and Leary, 1976) have usually assumed water budgets that allow for no mesoscale air motions. The results of such studies are correct only to the extent that they are insensitive to the neglect of the mesoscale anvil air motions.

The purpose of the present paper is to test the sensitivity of diagnostic results to the inclusion or exclusion of anvil clouds and their associated mesoscale updrafts and downdrafts. We carry out this test using the first approach mentioned above by postulating an idealized mesoscale system with a precipitation pattern typical of mesoscale systems observed during GATE. The response of a diagnostic model similar to that of H is examined as various assumptions are made about the water budget of the idealized mesoscale system. Some of these assumptions allow mesoscale updrafts and downdrafts to be associated with the precipitating anvil cloud of the idealized system. From the response of the model in this ideal case, we can anticipate the types of differences that will be obtained in diagnostic studies when the assumptions of the diagnostic models allow for mesoscale motions to contribute to the diagnosed mass and heat transports. Johnson's (1980) results show that for mesoscale downdrafts the types of differences we expect are obtained.

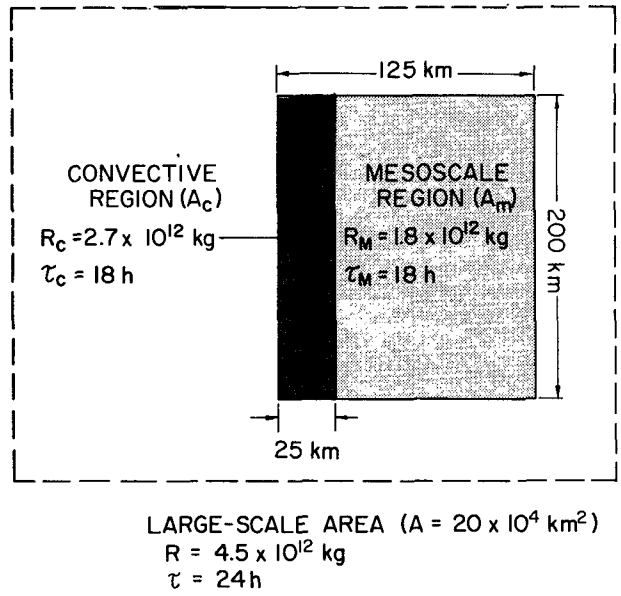

FIG. 1. Horizontal dimensions, lifetimes and rainfall for the components of the idealized mesoscale system and its larger scale environment. Symbols are defined in Section 2 of the text.

2. The idealized mesoscale system and three sets of assumptions about its water budget

The dimensions, lifetime and other characteristics of the mesoscale precipitation system, shown schematically in Fig. 1, were chosen to resemble most closely the squall-line system studied by Houze (1977), and to be consistent with the other systems described by Leary and Houze (1979a,b). The hypothetical system consists of a convective region of intense, cellular precipitation ($A_C = 0.5 \times 10^4$ km^2) and a mesoscale region of lighter, horizontally uniform rain ($A_M = 2.5 \times 10^4$ km^2). We specify a total lifetime (τ) of 24 h for this system and assume that, for the first 6 h, only the convective region is present, while for the last 6 h, only the mesoscale region is present. Thus, A_C and A_M each have lifetimes (τ_C and τ_M, respectively) of 18 h. The large-scale area ($A = 20 \times 10^4$ km^2) was chosen to represent the area occupied by the mesoscale system and its environment.

The vertical structure of the idealized mesoscale system is indicated in Fig. 2. In the case studied by Houze (1977), the precipitation in region A_C fell from cells which reached maximum heights of 10 to 17 km, with the bulk of the convective precipitation from cells of ~14 km. We assume here that all of the convective precipitation in region A_C fell from cells reaching a maximum height of z_T = 14 km. That is, our idealized system is assumed for mathe-

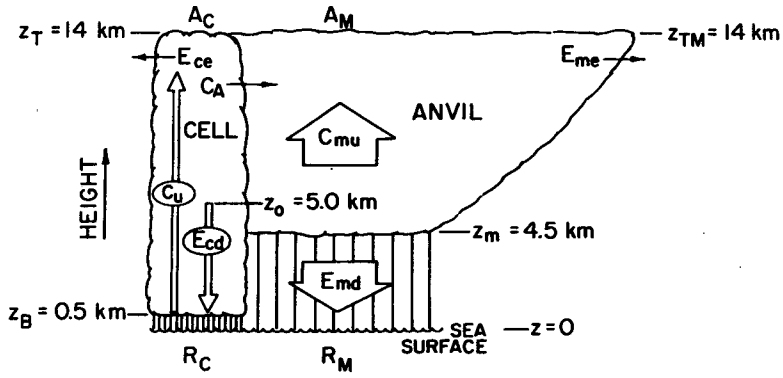

FIG. 2. Schematic vertical cross section of the idealized mesoscale system showing sources and sinks of condensed water. Symbols are defined in Section 2 of the text.

matical simplicity to have a spectrum containing convective cells of only one size. This assumption has no substantial effect on the results of this study, which is primarily concerned with how the anvil air motions are represented. Our results can easily be extrapolated to anticipate the results of diagnostic models (such as that of H) which allow for a spectrum of cells of various sizes. We assume further that the anvil cloud also has its top z_{Tm} at 14 km, while its base z_m is at 4.5 km. The convective cloud base z_B is assumed to be at 0.5 km, and the top of the convective downdraft z_0 is placed at 5.0 km.

The water budget of the mesoscale system is indicated schematically in Fig. 2. The water budget for the convective region can be expressed mathematically as

$$R_c = C_u - E_{cd} - E_{ce} - C_A \tag{1}$$

and for the mesoscale region as

$$R_m = C_{mu} - E_{md} - E_{me} + C_A, \tag{2}$$

where R_c and R_m are the total masses of rain (kilograms of water) which fall in regions A_C and A_M, respectively; C_u and C_{mu} are the masses of water condensed in convective updrafts in A_C and a mesoscale updraft in A_M, respectively; E_{cd} and E_{md} are the masses of water evaporated in convective downdrafts in A_C and a mesoscale downdraft in A_M, respectively; and E_{ce} and E_{me} are the amounts of water evaporated into the larger scale environment from A_C and A_M, respectively. C_A is the portion of C_u which is incorporated into the mesoscale region covered by the anvil cloud, either by being detrained, that is, advected horizontally into the anvil region by air flowing out of convective cells, or by being left aloft by cells which, upon dying, blend into the anvil cloud while new cells form ahead of the anvil region (Houze, 1977).

TABLE 1. Values of each term in the water budgets of Cases A, B and C, expressed as fractions of the total rainfall, R (4.5 × 10^{12} kg).

	$R_c = C_u - E_{cd} - E_{ce} - C_A$
Case A	0.6 = 1.30 − 0.17 − 0.09 − 0.44
Case B	0.6 = 1.75 − 0.23 − 0.12 − 0.80
Case C	0.6 = 1.25 − 0.16 − 0.09 − 0.40
	$R_m = C_{mu} - E_{md} - E_{me} + C_A$
Case A	0.4 = 0 − 0 − 0.04 + 0.44
Case B	0.4 = 0 − 0.32 − 0.08 + 0.80
Case C	0.4 = 0.40 − 0.32 − 0.08 + 0.40

We consider three possible water budgets for the mesoscale system by considering three different combinations of the values of the terms in (1) and (2). These values are listed in Table 1 and shown schematically in Fig. 3.

In each of the three water budgets, we assume a total mass of rain which falls from the system [R = 4.5 × 10^{12} kg, a value chosen to correspond to the squall-line system studied by Houze (1977)] with 60% falling in A_C and 40% falling in A_M. Thus, R_c = 0.6R and R_m = 0.4R. The mesoscale rain R_m, which falls in A_M, can be generated in two ways. Either water is first condensed in A_C and subsequently incorporated into A_M [term C_A in (1) and (2)], or the mesoscale rain in A_M is generated by mesoscale lifting [term C_{mu} in (2)], as in Brown's (1979) model. In the three cases examined here, the mesoscale rain in R_m is produced by three different combinations of C_A and C_{mu}.

As a further aid in comparing the three water budgets, eight parameters expressing ratios of various terms in (1) and (2) were chosen. Their mathematical definitions and values for each of the three cases are listed in Table 2. As discussed in H, these definitions, together with (1) and (2), imply that

$$\alpha + \beta + \eta + \nu_c = 1, \tag{3}$$

$$a + b + \nu_m = 1. \quad (4)$$

Three parameters of the water budget [α, β and b (Table 2)] were specified to be the same in each of the three cases, in order not to obscure the purpose of the calculations of mass and heat fluxes, namely, to test their sensitivity to different assumptions about mesoscale vertical air motions.

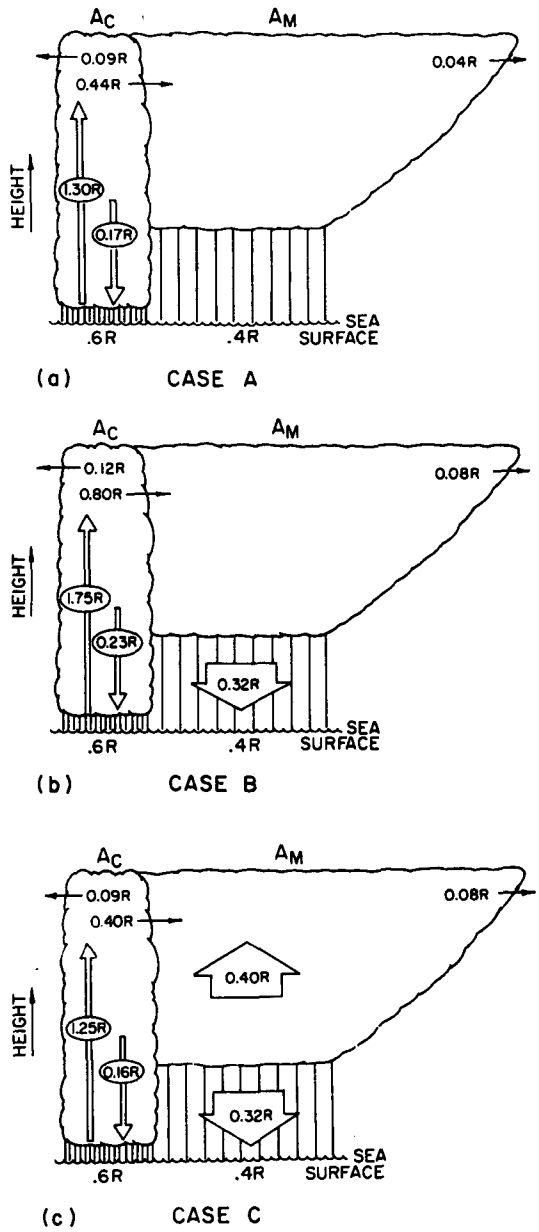

FIG. 3. Schematic vertical cross sections of the idealized mesoscale system showing values of terms in the water budget (cf. Fig. 2 and Table 1) for three different sets of assumptions: (a) convective-scale updrafts and downdrafts only (Case A); (b) convective-scale updrafts and downdrafts and a mesoscale downdraft (Case B); (c) convective-scale updrafts and downdrafts, a mesoscale updraft and a mesoscale downdraft (Case C).

TABLE 2. Definitions and values of water budget parameters.

Water budget parameters	Case A	Case B	Case C
$\nu_c = \frac{R_c}{C_u}$	0.46	0.34	0.48
$\alpha = \frac{E_{cd}}{C_u}$	0.13	0.13	0.13
$\beta = \frac{E_{ce}}{C_u}$	0.07	0.07	0.07
$\eta = \frac{C_A}{C_u}$	0.34	0.46	0.32
$\nu_m = \frac{R_m}{C_{mu} + C_A}$	0.90	0.50	0.50
$a = \frac{E_{md}}{C_{mu} + C_A}$	0	0.40	0.40
$b = \frac{E_{me}}{C_{mu} + C_A}$	0.10	0.10	0.10

The parameter α is the fraction of the convective condensate C_u reevaporated in convective downdrafts. In the controlled experiment of H, a value of $\alpha \approx 0.1$ was deduced for large convective clouds such as those assumed to be present in region A_C of our hypothetical mesoscale system. In the study of Houze and Leary (1976), reasonable diagnostic results were obtained with a value of $\alpha = 0.13$. In the present study, we again use the value $\alpha = 0.13$.

We arbitrarily assume that $\beta = 0.07$ and $b = 0.10$; i.e., 7% of the convective condensate and 10% of the anvil cloud condensate are reevaporated in the large-scale environment of the hypothetical mesoscale system. Storage of evaporated condensate in the environment undoubtedly occurs because clouds are usually observed in dissipating mesoscale systems after precipitation stops. In the absence of quantitative data, we assign this process a minor role in the water budgets of the convective and mesoscale regions.

a. Case A

Case A (Fig. 3a, Tables 1 and 2) assumes that R_m is accounted for entirely by C_A and there is no upward motion or condensation in the anvil cloud. Accordingly,

$$C_{mu} = 0. \quad (5)$$

It is further assumed that there is no mesoscale downdraft below the anvil, and hence no evaporation of condensate below the anvil. Thus,

$$E_{md} = 0. \quad (6)$$

Although these assumptions, which neglect mesoscale motions, seem unrealistic in view of the ob-

servations and modeling of mesoscale systems cited in the Introduction, they correspond to the basic assumptions of most convective parameterization schemes and previous diagnostic studies, namely, that all condensation and precipitation results from convective-scale motions alone. In particular, these assumptions were made in the controlled experiment of H, in which agreement was obtained between cloud population properties diagnosed from synoptic and radar data. By comparing the results of Case A with the results of the other two cases considered in this paper, which do take into account the effects of mesoscale as well as convective-scale motions, we can test the sensitivity of diagnostic results to the incorporation of mesoscale motions into diagnostic models.

Eqs. (5) and (6), together with the assumptions common to all three cases, are sufficient to completely define all the terms and parameters of the water budget in Case A. It follows from (6) that $a = 0$. Since $b = 0.1$, Eq. (4) implies that $\nu_m = 0.90$. From this value of ν_m and the fact that C_{mu} is zero, C_A is determined using the expression for ν_m in Table 2. Physically, the value of C_A thus determined is the amount of condensate that must be incorporated into the anvil region A_M from the convective region A_C in order to provide all of the water needed to account for R_m and E_{me} without having any condensation in the anvil itself. Since C_A is so determined and R_c is given, the ratio η/ν_c is determined using the expressions for η and ν_c in Table 2. Since ν_c, α, β and η must sum to unity to satisfy (3), and α and β are prescribed, the sum of ν_c and η must be 0.8. Since both the ratio and the sum of ν_c and η are known, both ν_c and η are determined.

b. Case B

In Case B (Fig. 3b, Tables 1 and 2), mesoscale lifting in the anvil is again precluded by assuming that C_{mu} is zero [i.e., Eq. (5) also applies in this case]. However, a mesoscale downdraft below the anvil is included and, consequently, evaporation of condensate occurs below the anvil. Rather than assuming a specific value for E_{md}, we specify that 40% of the condensate in the anvil (C_A) is evaporated in the mesoscale downdraft below the anvil. That is, we set $a = 0.40$ (Table 2). The choice of 40% for this assumption is discussed further in Section 3d.

Other details of the Case B water budget, summarized in Tables 1 and 2 and Fig. 3b, follow from the same line of reasoning described above for Case A.

c. Case C

Case C (Fig. 3c, Tables 1 and 2) is the most general case we consider. It has both mesoscale lifting in the anvil and a mesoscale downdraft below the anvil. Consequently, both C_{mu} and E_{md} are non-zero. As in Case B, we specify that 40% of the condensate in the anvil is evaporated in a mesoscale downdraft below the anvil. In Case C, however, anvil condensate has two sources, C_{mu} and C_A. In the absence of direct measurements to establish their relative contributions to the anvil condensate, we assume that

$$C_{mu} = C_A. \tag{7}$$

Physically, we are assuming that half of the condensate in the anvil cloud is condensed in the mesoscale updraft there, and that half of the condensate is transported from region A_c, where it was condensed in convective updrafts.

Using (7) it is possible to evaluate the other terms and parameters in the water budget for Case C (Tables 1, 2) using the same reasoning as for Cases A and B.

While there are no rigorous quantitative water budget studies that verify which of the three cases A–C is most realistic, it is evident that Case C is qualitatively the most reasonable of the three. The studies of Zipser (1969, 1977), Betts *et al.* (1976), Houze (1977), Zipser and Gautier (1978) and Leary and Houze (1979b) indicate from aircraft and synoptic data that mesoscale downdrafts do indeed occur below the anvil clouds of tropical cloud systems similar to the one considered here and that considerable evaporation occurs in these downdrafts. The large amount of rain from the anvil and the long life of anvil rain after convective cells became inactive further suggests the presence of a mesoscale updraft in the anvil itself. A persistent mesoscale updraft in the anvil cloud occurs in Brown's (1979) numerical simulation of a tropical squall-line system, and Ogura and Liou (1980) have observed both mesoscale updraft and downdraft in an Oklahoma squall line that resembled a tropical squall system. For all these reasons, we consider Case C to be the most realistic of the three postulated cases.

3. Calculations of the vertical fluxes of mass and moist static energy by the idealized mesoscale system

a. General relationships

The vertical mass flux over the large-scale area A during time τ (Fig. 1) can be expressed as

$$\bar{M} = M_e + M_u + M_d + M_m, \tag{8}$$

where the terms on the right side of the equation are contributions to $\bar{M}$ of vertical air motions in the large-scale environment (M_e), convective-scale updrafts (M_u) and downdrafts (M_d) in the convective region A_c, and mesoscale vertical air motions (M_m) in the mesoscale region A_M (Fig. 1). For our idealized case, we are concerned with the cloud contribution to $\bar{M}$, which may be written as

$$M = M_u + M_d + M_m. \tag{9}$$

The contribution to M from vertical air motions in the mesoscale region is due to the mesoscale updraft above the 4.5 km level and to the mesoscale downdraft below 4.5 km (Fig. 5). Hence, we have

$$M_m = \begin{cases} M_{mu}, & 4.5 \leq z \leq 14 \text{ km} \\ M_{md}, & 0 \leq \quad z < 4.5 \text{ km}, \end{cases} \tag{10}$$

where M_{mu} and M_{md} are the contributions to M of mass fluxes in the mesoscale updraft and downdraft, respectively.

Associated with M is a vertical eddy flux of moist static energy (which we sometimes refer to simply as the heat flux) over area A during time τ, which can be written as

$$F = F_u + F_d + F_m, \tag{11}$$

where F_u and F_d are the respective contributions of the convective-scale updrafts and downdrafts in region A_C, and F_m is the contribution of the mesoscale vertical air motions in region A_M (Fig. 1). These fluxes are given by

$$F_u = M_u(h_u - h_e), \tag{12}$$

$$F_d = M_d(h_d - h_e), \tag{13}$$

$$F_m = M_m(h_m - h_e), \tag{14}$$

where h is the moist static energy, defined as

$$h = c_pT + Lq + gz. \tag{15}$$

The subscripts u, d and m, when applied to h, refer, as in all other terms, to values computed for the convective-scale updrafts and downdrafts and the mesoscale anvil region, respectively. The subscript e refers to the large-scale environment, which is assumed to be that observed during Phase III of GATE, c_p is the specific heat at constant pressure, T temperature, L the latent heat of vaporization, q the water vapor mixing ratio and g the gravitational acceleration. Eq. (11), with substitution from (12)–(15), constitutes a special case of (H59),[3] where, in the notation of H, $F = -g^{-1}\widetilde{\overline{\omega' h'}}$, and the only clouds contributing to the heat flux are those comprising the idealized mesoscale system.

The methods used to calculate the mass fluxes (M_u, M_d and M_m) and moist static energies (h_u, h_d and h_m) appearing in (12)–(14) are discussed in the following subsections.

b. Convective updraft properties

The contribution to M by convective-scale updrafts is calculated from

$$M_u = \frac{\mu_B f_u(\lambda,z)}{A\tau}, \tag{16}$$

where μ_B is the mass of air transported through cloud base and $f_u(\lambda,z)$, in the notation of H, is the vertical profile of the convective updraft mass flux in convective cells with entrainment rate λ. Since the convective clouds in the idealized mesoscale system are all the same size (14 km in height), we assume the constant value

$$\lambda = 0.01 \text{ km}^{-1}, \tag{17}$$

which is the value used in the controlled experiment of H for clouds with tops at 14 km. This value is quite small. Because of their large size, the convective clouds in the idealized mesoscale system are essentially undilute "hot towers" (Riehl and Malkus, 1958). The profile used for $f_u(\lambda,z)$ is Cheng and Houze's (1980) adaptation of the profile used by Austin and Houze (1973) and Houze and Leary (1976).

The quantity μ_B is calculated from

$$\frac{R_c}{\nu_c} = I_1(\lambda)\mu_B, \tag{18}$$

where

$$I_1(\lambda) = \int_{z_B}^{z_T} f_u(\lambda,z)\left[\lambda(q_e - q_u) - \frac{\partial q_u}{\partial z}\right]dz. \tag{19}$$

Eq. (18) states that the amount of mass transported through cloud base μ_B is related to the convective rain R_c. It is a special case of Austin and Houze's (1973) Eq. (6) and (H36). In the notation of H, $\mu_B = \mathcal{M}_B(\lambda)d\lambda$, $R_c = R_c(\lambda)d\lambda$ and $\nu_c = \nu_c(\lambda)$ for $\lambda = 0.01$ km^{-1} [Eq. (17)]. The expression for the integral $I_1(\lambda)$ given by (19) is a special case of (H37).

The moist static energy in the convective updrafts is calculated from (H11) using the boundary condition that the air at the base of the updraft is saturated at the virtual temperature of the environment (Cheng and Houze, 1980). The temperature (T_u) and mixing ratio (q_u) in the convective updrafts are calculated from (H12) and (H13).

c. Convective downdraft properties

The contribution to M from convective-scale downdrafts is computed using

$$M_d = \frac{\mu_0 f_d(\lambda,z)}{A\tau}, \tag{20}$$

where μ_0 is the mass of air transported downward at the top of the downdraft (level z_0 in Fig. 2) and $f_d(\lambda,z)$ is the vertical profile of the convective downdraft mass flux in convective cells with entrainment rate λ. Following the procedures described in H, we assume the downdrafts have the same entrainment rate as the updrafts [Eq. (17)], and that z_0 is 5.0 km. The profile used for $f_d(\lambda,z)$ is Cheng and Houze's (1980) inverted version of the updraft profile $f_u(\lambda,z)$.

[3] Equations in H are denoted with the prefix H.

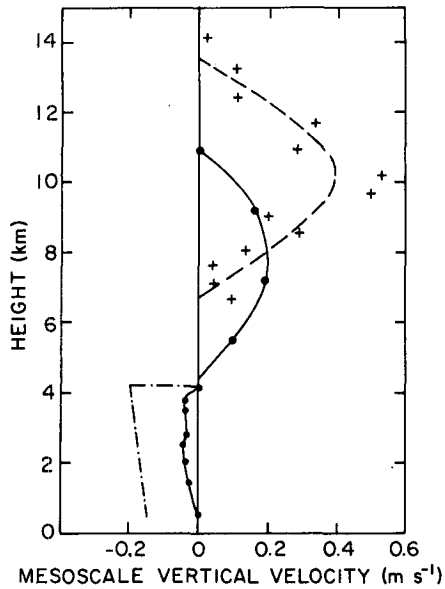

FIG. 4. Mesoscale vertical velocity profiles obtained from Brown's (1979) model results (black dots and solid line), from rawinsonde data (crosses and dashed line), and from Leary's (1979) one-dimensional mesoscale downdraft model (dash-dotted line).

The mass transported downward at the top of the downdraft μ_0 is calculated from

$$\mu_0 = \epsilon(\lambda)\mu_B, \tag{21}$$

where, following H,

$$\epsilon(\lambda) = \frac{\alpha I_1(\lambda)}{I_2(\lambda)}, \tag{22}$$

$$I_2(\lambda) = \int_0^{z_0} f_d(\lambda,z)\left[\lambda(q_e - q_d) + \frac{\partial q_d}{\partial z}\right]dz. \tag{23}$$

Eqs. (21)–(23) are special cases of (H41), (H42) and (H39), respectively, in which $\mu_0 = \mathcal{M}_0(\lambda)d\lambda$.

The moist static energy in the convective downdrafts is calculated from (H21), using the boundary condition that the air at the top of the downdraft is saturated at the wet-bulb temperature of the environment (Cheng and Houze, 1980). The temperature and mixing ratio in the convective downdrafts T_d and q_d are calculated from (H12) and (H13).

d. Mesoscale updraft and downdraft properties

The contributions to M of the mesoscale updraft and downdraft are expressed by

$$M_{mu} = \frac{\mu_{mu}(z)}{A\tau}, \tag{24}$$

$$M_{md} = \frac{\mu_{md}(z)}{A\tau}, \tag{25}$$

where $\mu_{mu}(z)$ and $\mu_{md}(z)$ are the masses of air transported vertically through level z in the mesoscale updraft and downdraft, respectively. The following paragraphs explain how M_{mu} and M_{md}, as well as the moist static energy h_m, are determined for the idealized mesoscale system.

Insight for constructing a mesoscale updraft profile is sought first in the results of Brown's (1979) model. A profile of the average vertical velocity in the anvil cloud found downshear of his line of convective updrafts is shown by the solid line above 4 km in Fig. 4.

Since the heights of convective clouds are limited by the assumptions of his model, his profile for the mesoscale updraft appears at lower levels than would be realistic in our case, in which convective updrafts reach a height of 14 km. The shape of his profile, and the maximum value of the updraft (0.2 m s^{-1}) do, however, provide useful guidance for constructing a plausible profile for our case.

Another estimate of the profile of vertical velocity in a mesoscale updraft was obtained from vertical profiles of the wet-bulb potential temperature θ_w obtained from rawinsonde observations 3 h apart in the mesoscale region of the squall-line system described by Houze (1977). This estimate was obtained by substituting θ_w for ξ in (H26). We note that θ_w is conserved and assume that there is no storage of θ_w. Hence, the terms S_m and $\mathcal{S}_m$ in (H26) disappear. Then, combining (H26) and (H28), we obtain

$$w_m = -\frac{(\mathbf{V}_R)_m\cdot(\nabla\theta_w)_m}{\left(\dfrac{\partial\theta_w}{\partial z}\right)_m}, \tag{26}$$

where, in the notation of H, $\mathbf{V}_R$ is the horizontal wind relative to the mesoscale system, and the m indicates an average over the lifetime and area covered by the mesoscale anvil region. If it is further assumed that the θ_w field moving with the system is two-dimensional and steady-state, Eq. (26) becomes

$$w_{mu} = \frac{\dfrac{U_R}{U_S}\left(\dfrac{\partial\theta_w}{\partial t}\right)_m}{\left(\dfrac{\partial\theta_w}{\partial z}\right)_m}, \tag{27}$$

where U_R is the component of $\mathbf{V}_R$ normal to the squall line, $\partial\theta_w/\partial t$ is the local time derivative resulting from the passage of the steady-state θ_w field over a point fixed to the earth, and U_S is the speed of the system.[4] The subscript mu is used to indicate that here we are only concerned with the value of the vertical velocity in the mesoscale updraft. The ratio of relative wind velocity to squall-line propagation

[4] The sign convention is that U_S is always positive, but U_R is negative if it is directed against U_S.

speed as a function of height was obtained using the analyses of Houze (1977, Figs. 5, 7 and 15) and the *Oceanographer* sounding taken at 1800 on 4 September 1974. That sounding was also used to estimate $(\partial\theta_w/\partial t)_m$. Values of $(\partial\theta_w/\partial z)_m$ were calculated using the 1800 and 2100 soundings from the *Oceanographer*. Only the 1800 sounding was used to calculate U_R/U_S and $(\partial\theta_w/\partial z)_m$. The wind observations at 2100 were noisy and thus not reliable for calculating U_R and, being taken at the outer edge of the anvil cloud, the thermodynamic data for 2100 did not give a representative value of $(\partial\theta_w/\partial z)$ centered on the mesoscale anvil region.

The vertical velocity profile computed from (27) is shown by the crosses and dashed line in Fig. 4. The shape of the curve for our observed squall-line system is consistent with Brown's results. The greater height and larger maximum magnitude (~0.4 m s^{-1}) of our velocity maximum compared to the profile derived from Brown's (1979) model is in keeping with the greater height and probably greater intensity of the convective cells in our case.

Based on the shapes of the profiles of vertical velocity in the mesoscale updraft shown in Fig. 4, we have chosen a parabolic profile for the vertical velocity within the mesoscale updraft of our hypothetical mesoscale system. The parabolic profile, with its maximum magnitude equal to 1.0 at $z' = 10$ km, is illustrated in Fig. 5 and is referred to as $f(z)$. The vertical velocity in the mesoscale updraft is then given by

$$w_{mu}(z) = w_{mu}(z')f(z), \tag{28}$$

and (24) can be written in the form

$$M_{mu} = \frac{\rho_{mu}(z)w_{mu}(z')A_m\tau_m f(z)}{A\tau}, \tag{29}$$

where $\rho_{mu}(z)$ is the density of the air at height z in the mesoscale updraft.

The magnitude of $w_{mu}(z')$ in (29) was calculated for the water budget of Case C (the case described in Section 2 that contains a mesoscale updraft) using the equation for the continuity of water vapor in the mesoscale updraft. This equation is obtained by substituting the water vapor mixing ratio q for ξ in (H26) and assuming that the effects of storage ($\mathcal{S}_m$) and horizontal advection ($\mathcal{H}_m$) of q are small compared with sources and sinks (S_m). Then, (H26) becomes

$$\frac{dq_m}{dz} = S_m. \tag{30}$$

It is further assumed that condensation is the only significant contribution to S_m. The evaporation of anvil cloud water represented by E_{me} is a source of vapor for the large-scale environment, not the anvil. Hence, it does not contribute to S_m. Integration of

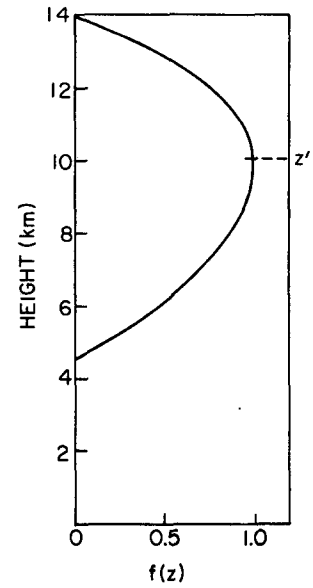

FIG. 5. Parabolic profile of vertical velocity chosen for the mesoscale updraft.

(30) over the depth of the mesoscale updraft leads to

$$w_{mu}(z') = \frac{-C_{mu}}{A_M\tau_m \int_{z_m}^{z_{Tm}} \rho_{mu}f(z)\dfrac{dq_m}{dz}\,dz}, \tag{31}$$

which is analogous to (H50).[5]

The density ρ_{mu}, dq_m/dz in (31), and the value of h_m in the mesoscale updraft heat flux in (14) are all specified for the mesoscale updraft by assuming that the mesoscale updraft is saturated and 1 K higher in temperature than the large-scale environment. This value was chosen on the basis of the results of Brown's (1979) model and is consistent with the observations of Zipser (1969, 1977), Betts *et al.* (1976) and Houze (1977) who show that the moist-static energy of the air flowing out of the anvils of tropical squall lines is higher than it is at the same levels in the large-scale environment ahead of the lines.

With these assumptions, $w_{mu}(z')$ for Case C was calculated from (31) to be 0.5 m s^{-1}, and this value was substituted into (29) to obtain M_{mu}. The value of $w_{mu}(z')$ obtained from (31) is directly proportional to the value of C_{mu}, which for Case C is given by (7). Since the value obtained (0.5 m s^{-1}) slightly exceeds the other estimates of $w_{mu}(z')$ (0.2 m s^{-1} from Brown's model and 0.4 m s^{-1} from Houze's θ_w cross section), it appears that the value of C_{mu} given by (7) is of the right order of magnitude, but is probably

[5] In (H50), the integral I_3 is written in terms of the *mass flux* profile $f_{mu}(z)$, while the integral in (31) is written in terms of the *vertical velocity* profile $f(z)$.

TABLE 3. Vertical profiles of temperature, density, moisture and vertical velocity in the mesoscale downdraft (from Leary, 1980, Fig. 4) used for the calculations described in Section 3.

Pressure (mb)	Density (kg m^{-3})	Height (m)	Temperature (K)	Water vapor mixing ratio ($\times 10^{-3}$)	Relative humidity (%)	Downdraft speed (m s^{-1})
618	0.785	4163	273.16	6.21	100	0.200
625	0.792	4072	274.03	6.22	95	0.198
650	0.816	3753	276.61	6.45	85	0.193
675	0.840	3445	278.68	6.84	81	0.187
700	0.866	3146	280.51	7.29	79	0.181
725	0.891	2855	282.16	7.78	78	0.176
750	0.916	2572	283.70	8.29	77	0.171
775	0.942	2297	285.16	8.79	77	0.167
800	0.967	2030	286.56	9.30	76	0.162
825	0.992	1769	287.92	9.79	76	0.158
850	1.017	1515	289.27	10.26	75	0.154
875	1.042	1268	290.64	10.70	74	0.151
900	1.067	1026	291.92	11.15	73	0.147
925	1.092	789	293.15	11.60	72	0.144
950	1.116	558	294.34	12.05	71	0.141
955	1.121	512	294.58	12.14	71	0.140

an upper limit. Since Cases A and B assume that $C_{mu} = 0$, our calculations for Cases A, B and C can be considered to cover the probable range of mesoscale updrafts, and these are indicated to have maximum magnitudes in the range from 0 to 0.5 m s^{-1}.

In order to compute M_{md}, it is necessary to obtain a vertical profile of vertical velocity or mass flux in the mesoscale downdraft. The average vertical velocity in the mesoscale downdraft below the anvil in Brown's model is shown by the solid line below 4 km in Fig. 4. Zipser (1977) estimated a mean sinking rate of 0.05–0.25 m s^{-1} at an altitude of 500 m in mesoscale downdrafts, based on soundings obtained beneath anvils. For our calculations, we use the vertical velocity profile and thermodynamic properties in the mesoscale downdraft shown by the dot-dashed line in Fig. 4 and listed in Table 3. Leary (1980) obtained these values by constructing a one-dimensional downdraft model capable of producing temperature and moisture profiles similar to those observed by Zipser (1977) and Houze (1977).

Her model assumes that some combination of subsidence, which warms and dries the air, and evaporation of rain falling from the anvil, which cools and moistens the air, can be found that explains the observed temperature and humidity profiles in the downdraft region. A size distribution of raindrops, based on particle size measurements obtained in GATE, is postulated, and the rate of evaporation of the drops is computed microphysically. The amount of subsidence required to offset the evaporation just enough to give ambient temperature and humidity profiles similar to those observed below anvils is assumed to approximate the true mesoscale downdraft.

Leary's results were used to determine M_{md} by writing (25) as

$$M_{md} = \frac{\rho_{md}(z) w_{md}(z) A_m \tau_m}{A\tau}, \tag{32}$$

and using her values of the density $\rho_{md}(z)$ and $w_{md}(z)$ given in Table 3.

Alternatively, M_{md} can be expressed as

$$M_{md} = \frac{\mu^*_{md} f_{md}(z)}{A\tau}, \tag{33}$$

where $f_{md}(z)$ is the non-dimensional, normalized mass flux profile for the mesoscale downdraft (see Section 2d of H) and μ^*_{md} is the mass transported through the level (or levels) where $f_{md}(z) = 1$. In Leary's calculations, it is assumed that there is a constant downward mass flux between the top of the downdraft at 618 mb (4.2 km) and its base at 955 mb (0.5 km). Therefore, in (33)

$$f_{md}(z) = \begin{cases} 1, & 0.5 \text{ km} \leq z \leq 4.2 \text{ km} \\ 0, & \text{otherwise.} \end{cases} \tag{34}$$

The quantity μ^*_{md} in (33) is related to the parameters of the water budget of the mesoscale region [Eq. (H56)]. Substituting from (H56), Eq. (33) becomes

$$M_{md} = \frac{a R_m f_{md}(z)}{I_4 \nu_m A\tau}. \tag{35}$$

I_4 can be determined from (H55) with $f_{md}(z)$ given by (34) and q_{md} by Table 3. Using the value of M_{md} obtained from (32), two unknowns remain in (35), a and ν_m. The same two unknowns are in (4) (since b is assumed to be 0.1). Simultaneous solution of (4) and (35) leads to the values of $a = 0.4$ and $\nu_m = 0.5$. Thus, the value of M_{md} obtained from (32)

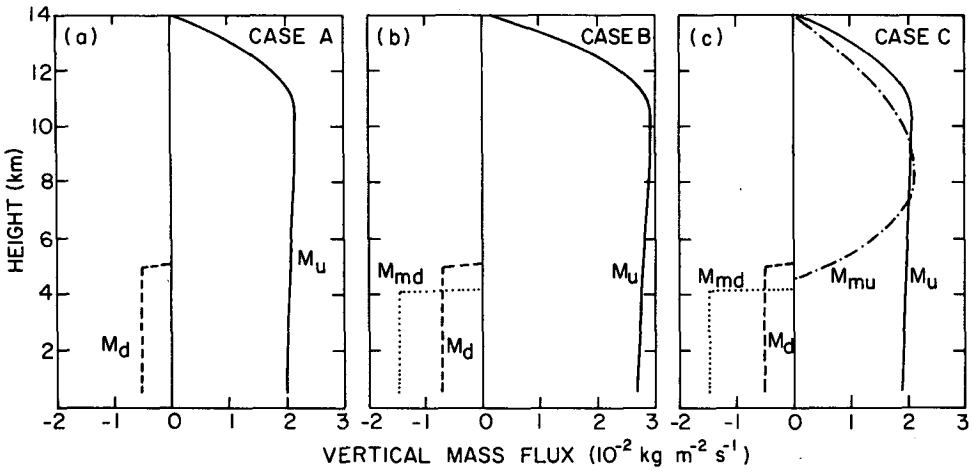

FIG. 6. Contributions to M, the cloud vertical mass flux averaged over the large-scale area A during time τ, due to convective-scale updrafts (M_u) and downdrafts (M_d), a mesoscale updraft (M_{mu}), and a mesoscale downdraft (M_{md}) in the idealized mesoscale system for (a) Case A, (b) Case B and (c) Case C.

is the same as the value that would be obtained from (35) by assuming the water budgets for Cases B and C given in Tables 1 and 2. Leary's (1980) calculations, however, give a physical basis to these assumptions, which would otherwise have to be made *ad hoc*.

In addition to the mass flux calculation just described, the heat flux associated with the mesoscale downdraft was computed from (14) using the value of h_m derived from the data in Table 3.

4. Results

Figs. 6 and 7 show contributions to the vertical fluxes of mass and moist static energy, respectively, by cumulus and mesoscale motions for each of the three assumed water budgets. The vertical mass flux in convective-scale updrafts and downdrafts is directly proportional to the total amount of water condensed in region A_C. Since Case B (Fig. 6b), with a mesoscale downdraft but no mesoscale updraft, produces the most condensate in A_C, it has the greatest convective-scale mass transports. Likewise, Cases A (Fig. 6a) and C (Fig. 6c), with nearly equal but successively smaller amounts of condensation in A_C, have nearly equal but successively smaller vertical mass fluxes due to convective-scale updrafts and downdrafts.

The mesoscale downdraft in Case B makes a negative contribution to the vertical mass flux

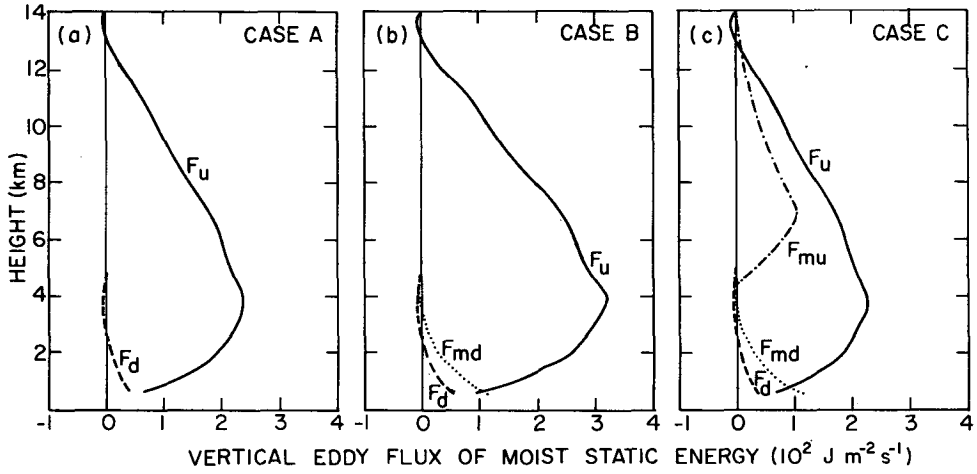

FIG. 7. Contributions to F, the vertical eddy flux of moist static energy averaged over the large-scale area A during time τ, due to convective-scale updrafts (F_u) and downdrafts (F_d), a mesoscale updraft (F_{mu}), and a mesoscale downdraft (F_{md}) in the idealized mesoscale system for (a) Case A, (b) Case B and (c) Case C.

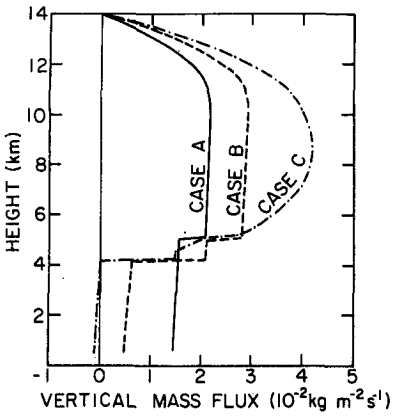

FIG. 8. Vertical profiles of M, the cloud vertical mass flux averaged over the large-scale area A during time τ, due to both convective-scale and mesoscale vertical air motions in the idealized mesoscale system for Cases A, B and C.

approximately twice that of the convective-scale downdrafts. In Case C the mesoscale downdraft makes about three times as great a contribution to the total mass transport as the convective-scale downdraft. Since the vertical velocity for the mesoscale downdraft in Cases B and C is the same, the fluxes of mass and moist static energy due to the mesoscale downdraft are the same for both cases.

The mesoscale updraft in Case C makes a positive contribution to the vertical flux of mass similar in magnitude to that of the convective-scale updrafts above 6 km.

Since M_u is largest in Case B, F_u is also largest for Case B (Fig. 7b). Likewise, Cases A (Fig. 7a) and C (Fig. 7c) have nearly equal but successively smaller values of F_u at each level. At high levels, near 14 km, cumulus updrafts that penetrate the stable layer near the tropopause have small negative values of F_u. In Case C these negative values of F_u are partially offset by small positive values of F_{mu} near 14 km. Because the magnitude of F_{cd} is directly proportional to M_{cd}, Case B (Fig. 7b) again shows the greatest convective-scale heat flux and Case C (Fig. 7c) the least. The convective-scale downdraft, colder but at higher levels moister than the environment, makes F_d positive near cloud base and slightly negative above 2.8 km. The mesoscale downdraft is colder and drier than the environment at all levels except those just below the top of the downdraft, where the negative contribution of F_m is very small. At levels near cloud base, F_m makes a positive contribution to F more than double that of the convective-scale downdrafts in Cases B (Fig. 7b) and C (Fig. 7c).

The contribution of the mesoscale updraft to the vertical eddy flux of moist static energy (Fig. 7c) is comparable to but smaller than that of the convective-scale updrafts because the convective-scale updrafts are warmer and moister than the mesoscale updraft.

Fig. 8 shows the total vertical flux of mass for Cases A, B, and C, calculated as the total of the contributions from all convective-scale and mesoscale motions. Cases B and C, which include mesoscale as well as convective-scale motions, show larger mass transports in the upper troposphere and smaller mass fluxes in the lower troposphere than does Case A, which assumes that all of the cloud vertical motions are of convective scale. Case C, which has both a mesoscale updraft and a mesoscale downdraft, shows the largest mass flux of all in the upper troposphere (above 5 km), and the smallest in the lower troposphere. In fact, M is slightly negative below 4 km in Case C. Case A, without a mesoscale downdraft, has the largest M below 3.8 km. In Case B, the presence of a mesoscale downdraft is partially offset by the larger values of M_{cu} than in the other two cases. These results imply that calculations which do not include the mesoscale vertical air motions in intense tropical convection might overestimate the cloud mass flux at low levels and underestimate it at upper levels.

In his diagnostic calculations based on heat budgets (i.e., the synoptic approach, in the terminology of H), Johnson (1980) also finds that inclusion of mesoscale downdrafts results in significantly smaller cloud mass fluxes at lower levels than when only convective-scale mass fluxes are included. Our results further show that when mesoscale updrafts as well as mesoscale downdrafts are included (Case C), the cloud mass fluxes at low levels are further reduced. With a mesoscale updraft, a significant portion (C_{mu}) of the total condensate is produced aloft in the anvil cloud without contributing to the cloud mass flux at low levels.

The total vertical eddy fluxes of moist static energy (F) for Cases A, B and C are shown in Fig. 9. Relatively little difference in the three curves can be seen above 10 km. Although the mass transports are greater at these upper levels in Case C (Fig. 8), little effect is produced in the profile of F since the mesoscale updraft is less effective than the convective-scale updrafts in transporting moist static energy upward. The difference in F from Case B to Case A above 5.1 km is directly proportional to the difference in M_{cu} between those cases.

Striking differences in shape and magnitude exist among the three profiles of F below 10 km. The peak in F for Case C (Fig. 9) is higher than the peaks for Cases A and B (6.5 km compared to 3.5 km). This reflects the presence of the mesoscale updraft in Case C, as the peak in F_{mu} occurs ~3 km higher than the peak in F_{cu} (Fig. 7c). Below 4.5 km, where the mesoscale updraft makes no contribution to F,

Case C exhibits significantly lower values of F than Case B, which possesses larger heat transports due to convective-scale updrafts than Case C.

In comparing the profiles of F in Fig. 9 below 10 km, differences in slope among the three cases are of particular interest since the slope of the profile, dF/dz, gives the cooling (positive slope) or heating (negative slope) rate associated with the vertical divergence of the cloud fluxes of moist static energy.

Between cloud base and 4.5 km, Case C exhibits no net heating. At the lowest levels the cooling accomplished by convective updrafts is balanced by heating in the mesoscale and convective downdrafts, while near 4 km, the slopes of F_{md}, F_c and F_u are all nearly zero (Fig. 7). Net cooling in the lower troposphere in Case C is restricted to the layer between 4.5 and 6.5 km, with net heating up to 13.5 km. Cases A and B, which lack a mesoscale updraft, show net cooling below 3.5 km and net heating up to 13.5 km. Compared to Case A, Case B exhibits less cooling in the layer between cloud base and 3.5 km because it possesses a mesoscale downdraft which partially compensates for the cooling due to convective updrafts. Since the slope of F_u is much greater in Case B than in Case C below 3.5 km (Fig. 7), the downdrafts cannot completely compensate for the cooling at low levels as occurs in Case C.

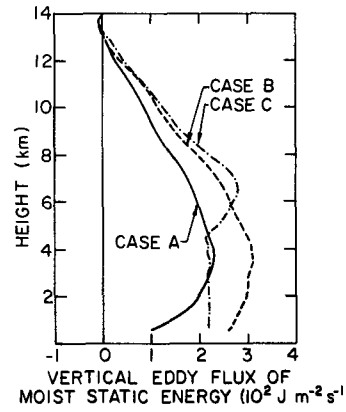

FIG. 9. Vertical profiles of F, the vertical eddy flux of moist static energy averaged over the large-scale area A during time τ, due to both convective-scale and mesoscale vertical air motions in the idealized mesoscale system for Cases A, B and C.

5. Conclusions

We have found, using estimates of the magnitudes of mesoscale vertical air motions, that mesoscale updrafts and downdrafts can make important contributions to the vertical fluxes of mass and moist static energy in intense tropical convection. Assuming three different water budgets for an idealized mesoscale system has enabled us to isolate the contributions to the total fluxes from convective-scale updrafts, convective-scale downdrafts, a mesoscale updraft and a mesoscale downdraft in three cases containing different combinations of these types of vertical motions but the same total amount of precipitation. Mesoscale air motions, where included in the calculations (Cases B and C), make contributions to the vertical transports of mass and moist static energy comparable in magnitude to those of their convective-scale counterparts. Inclusion of the mesoscale air motions, however, changes the vertical distributions of the computed mass and heat transports. Mass transport calculations which do not include the mesoscale motions produce larger mass fluxes in the lower troposphere and smaller mass transports in the upper troposphere than when the mesoscale motions are included. We find further that the heat flux associated with the mesoscale updraft leads to cooling in the layer between 4.5 and 6.5 km. Without the mesoscale updraft, the slope of the vertical flux profile is in the direction of net warming in this layer. Below 4 km, when both a mesoscale updraft and downdraft are included, the net heating is negligible because the mesoscale and convective-scale downdrafts are able to compensate for the cooling produced by the convective-scale updrafts.

The large differences in the mass and heat flux profiles obtained when our model water budget assumptions allowed mesoscale updrafts and downdrafts to contribute to the fluxes (Cases B and C) raises important questions about diagnostic methods and convective cloud parameterizations that make assumptions that suppress the mesoscale motions. Observational (Zipser, 1969, 1977; Betts *et al.*, 1976; Houze, 1977; Zipser and Gautier, 1978; Leary and Houze, 1979a,b; Cheng and Houze, 1979; Ogura and Liou, 1979) and theoretical (Brown, 1979) studies now indicate strongly that mesoscale drafts are significant components of tropical cloud populations. Consequently, if mesoscale vertical motions are suppressed in diagnostic models or parameterization schemes, by making either explicitly or implicitly the assumptions expressed by Eqs. (5) and (6), then convective-scale updrafts and downdrafts are required artificially to account for fluxes actually accomplished by the mesoscale motions. Our calculations in this paper suggest that diagnostic results obtained with models including assumptions allowing for mesoscale motions will be significantly more realistic.

Since the calculations of this paper closely follow the general diagnostic scheme outlined in H, we anticipate that the application of a diagnostic method, with model assumptions allowing for the contribution of mesoscale anvil air motions to mass and heat fluxes, will in fact lead to results qualitatively similar to those of our idealized mesoscale system.

Future studies should make use of synoptic mass, heat and moisture budgets as well as observed precipitation patterns and their radar-detected structure to determine how the mesoscale anvil motions within large cloud ensembles combine in their effects with the convective cells to satisfy large-scale budgets. One study (Johnson, 1980) of this type, dealing particularly with mesoscale downdrafts, has already been completed and is consistent with our results. Through studies of this type we can expect progress to be made toward the larger objective of whether mesoscale as well as convective-scale motions need to be accounted for in parameterization schemes for numerical models of the large-scale flow over the tropical oceans.

Acknowledgments. We thank C.-P. Cheng for his assistance with the computer program used to calculate the convective transports of mass and moist static energy. This research was supported by the Global Atmospheric Research Program, Division of Atmospheric Sciences, National Science Foundation and the GATE Project Office, National Oceanic and Atmospheric Administration, under Grants ATM74-14830 A01 and ATM78-16859.

REFERENCES

Abercromby, R., 1887: *Weather*. D. Appleton and Company, 472 pp. (see p. 248).

Austin, P. M., and R. A. Houze, Jr., 1973: A technique for computing vertical transports by precipitating cumuli. *J. Atmos. Sci.*, **30**, 1100–1111.

Betts, A. K., R. W. Grover and M. W. Moncrieff, 1976: Structure and motion of tropical squall-lines over Venezuela. *Quart. J. Roy. Meteor. Soc.*, **102**, 395–404.

Brown, J. M., 1979: Mesoscale unsaturated downdrafts driven by rainfall evaporation: A numerical study. *J. Atmos. Sci.*, **36**, 313–338.

Cheng, C.-P., and R. A. Houze, Jr., 1979: The distribution of convective and mesoscale precipitation in GATE radar echo patterns. *Mon. Wea. Rev.*, **107**, 1370–1381.

——, and ——, 1980: Sensitivity of diagnosed convective fluxes to model assumptions. *J. Atmos. Sci.*, **37**, 774–783.

Hamilton, R. A., and J. W. Archbold, 1945: Meteorology of Nigeria and adjacent territory. *Quart. J. Roy. Meteor. Soc.*, **71**, 231–262.

Houze, R. A., Jr., 1977: Structure and dynamics of a tropical squall-line system. *Mon. Wea. Rev.*, **105**, 1540–1567.

——, and C. A. Leary, 1976: Comparison of convective mass and heat transports in tropical easterly waves computed by two methods. *J. Atmos. Sci.*, **33**, 424–429.

——, C.-P. Cheng, C. A. Leary and J. F. Gamache, 1980: Diagnosis of cloud mass and heat fluxes from radar and synoptic data. *J. Atmos. Sci.*, **37**, 754–773.

Humphreys, W. R., 1914: The thunderstorm and its phenomena. *Mon. Wea. Rev.*, **42**, 348–380.

Johnson, R. H., 1976: The role of convective-scale precipitation downdrafts in cumulus and synoptic-scale interactions. *J. Atmos. Sci.*, **33**, 1890–1910.

——, 1980: A diagnostic model for cloud population properties that includes effects of convective-scale and mesoscale downdrafts. *J. Atmos. Sci.*, **37**, 733–753.

Leary, C. A., 1980: Temperature and humidity profiles in mesoscale unsaturated downdrafts. *J. Atmos. Sci.*, **37**, 784–796.

——, and R. A. Houze, Jr., 1979a: Melting and evaporation of hydrometeors in precipitation from the anvil clouds of deep tropical convection. *J. Atmos. Sci.*, **36**, 669–679.

——, and ——, 1979b: The structure and evolution of convection in a tropical cloud cluster. *J. Atmos. Sci.*, **36**, 437–457.

Ogura, Y., and H.-R. Cho, 1973: Diagnostic determinations of cumulus cloud populations from observed large-scale variables. *J. Atmos. Sci.*, **30**, 1276–1286.

——, and M.-T. Liou, 1980: The structure of a midlatitude squall line: A case study. *J. Atmos. Sci.*, **37**, 553–567.

Riehl, H., and J. S. Malkus, 1958: On the heat balance of the equatorial trough zone. *Geophysica*, **6**, 503–538.

Yanai, M., S. Esbensen and J.-H. Chu, 1973: Determination of the bulk properties of tropical cloud clusters from large-scale heat and moisture budgets. *J. Atmos. Sci.*, **30**, 611–627.

Zipser, E. J., 1969: The role of organized unsaturated convective downdrafts in the structure and rapid decay of an equatorial disturbance. *J. Appl. Meteor.*, **8**, 799–814.

——, 1977: Mesoscale and convective-scale downdrafts as distinct components of squall-line circulation. *Mon. Wea. Rev.*, **105**, 1568–1589.

——, and C. Gautier, 1978: Mesoscale events within a GATE tropical depression. *Mon. Wea. Rev.*, **106**, 789–805.